Fano resonance enhanced multiphoton photoemission from single plasmonic nanostructure excited by femtosecond laser

Guiqi Wang,[1] Xiaowei Song,[1] Meiling Jiang,[2] Peng Lang,[1] Boyu Ji,[1,*] Zheyu Fang,[2] and Jingquan Lin[1,†]
[1]*School of Science, Changchun University of Science and Technology, Changchun 130022, People's Republic of China*
[2]*School of Physics, State Key Lab for Mesoscopic Physics, Academy for Advanced Interdisciplinary Studies, Nano-Optoelectronics Frontier Center of Ministry of Education, Peking University, Beijing 100871, China*

(Received 2 December 2020; revised 23 February 2021; accepted 23 March 2021; published 5 April 2021)

High-flux photoelectron pulses with femto-nano spatiotemporal properties enhanced with plasmonic metallic nanostructures can provide possibilities for potential photoelectron-based devices. In this work, a large multiphoton photoemission enhancement in a single plasmonic Au-heptamer nanostructure, which supports the Fano resonance, is investigated using photoemission electron microscopy (PEEM). By exploiting the high spatial PEEM resolution and performing calculations, it is found that the photoemission electrons are mainly emitted from the junction area between the lower surface of the nanostructure and the indium tin oxide film on the substrate. It is also observed that photoemission is strongly affected by the Coulomb field. Specifically, the strong photoemission locates in the gap region with the Coulomb attraction rather than Coulomb repulsion, even though the latter exhibits a higher charge density. The measured photoelectron enhancement achieved by employing a Fano-resonant Au heptamer is supported by calculations, combining the photoemission effects of both near-field intensity in the lower surface and nanostructure absorption.

DOI: 10.1103/PhysRevB.103.155403

I. INTRODUCTION

Because of its localized near-field enhancement effects and optical response control at the nanometer scale, plasmon resonance has attracted significant attention and has been widely applied in the field of light-matter interaction in, for example, nonlinear optical systems, optoelectronics, and biochemical sensing [1,2]. Recently, the plasmon effects in metallic-nanostructure arrays have also been employed to improve the electron yield [3–9]. Even though the plasmon effects in a nanostructure array can greatly improve the electron yield of a metal, the large lateral size of these arrays, generally in the micrometer or even millimeter scale, will undoubtedly reduce the spatial resolution of a photoelectron-based device (e.g., a photocathode). As a result, the application of a photoelectron-based device to, for instance, high spatial and temporal resolution electron microscopy is restricted [10,11]. By utilizing plasmon-induced strong photoemission enhancement in a single nanostructure, the degraded spatial-resolution problem of an electron source can be eliminated.

It is known that the photoelectron yield induced by surface plasmons is closely related to the near-field enhancement and absorption [3,12]. The plasmonic Fano resonance, which is a plasmon mode induced by destructive interference between a "bright" mode and a "dark" mode, is capable of significantly reducing or even preventing the radiation damping pathway [13,14]. Reduced radiative damping in a Fano-resonant nanostructure will result in not only great near-field enhancement but also strong absorption around the Fano-resonant wavelength [15–17]. Therefore, achieving an improvement in the multiphoton photoemission yield in a Fano-resonant nanostructure is particularly important. However, to the best of our knowledge, the Fano resonance-enhanced multiphoton photoemission in a single plasmonic nanostructure has not yet been investigated.

In this work, the photoemission characteristics of plasmon Fano-resonant Au-heptamer nanostructures are investigated using photoemission electron microscopy (PEEM). PEEM has been a powerful tool for investigating near-field properties of plasmonic nanostructures [18–24]. It is found that the photoemission yield-enhancement factor of a Fano-resonant single nanostructure illuminated by a femtosecond laser can be up to six orders of magnitude higher than that of a gold flat surface, reaching the enhancement level of a plasmonic array [4] but with a greatly reduced lateral size of the photoelectron pulse. By exploiting the high spatial resolution of PEEM, it is deduced that the photoemission electrons are generated from the junction between the lower surface of the Au-heptamer nanostructure and the coated indium tin oxide (ITO) surface on the substrate rather than from the upper surface of the heptamer. More importantly, it is found that photoemission is strongly affected by the Coulomb field, and the strong photoemission locates in the gap region with the Coulomb attraction rather than Coulomb repulsion, even though the latter exhibits a higher charge density.

II. EXPERIMENTAL SETUP

Focus PEEM with a spatial resolution of 40 nm was employed to display photoelectron emission from a heptamer

*Corresponding author: jiboyu@cust.edu.cn
†Corresponding author: linjingquan@cust.edu.cn

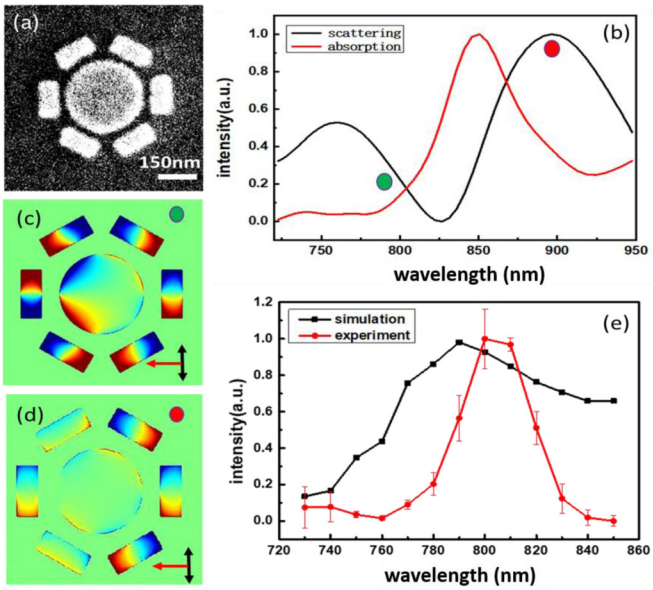

FIG. 1. (a) SEM image of the Au-heptamer structure. (b) Far-field scattering and absorption spectrum depicted by black solid and red solid lines, respectively, of the Au-heptamer nanostructure simulated using FDTD. Simulated charge distribution of the Au-heptamer nanostructure at (c) 790 nm and (d) 880 nm. The black and red arrows indicate the E and k vectors, respectively, which are the in-plane projections of the excitation field and its k vector. (e) Near-field spectrum of the Au-heptamer nanostructure obtained from PEEM (red line) and simulated near-field enhancement spectrum (black line) under s polarization light illumination. The simulated near field spectrum is obtained by integrating the electric field intensity within the whole structure.

nanostructure. In this experiment, a delay line detector was used to accurately acquire the number of photoemission electrons. A mode-locked Ti-sapphire laser oscillator (Coherent, Mira 900) capable of delivering 150-fs-duration laser pulses with a 76-MHz repetition rate and a tunable output wavelength in the range of 700–900 nm was used to excite the nanostructure. The sample was illuminated by an incident laser pulse at 65° with respect to the vertical axis of the sample. The bandwidth of the laser source was 12 nm. Details of the experimental setup have been reported in [25]. The heptamer sample consisted of a planar nanodisk monomer with a 125-nm radius placed in its center and six planar nanorods placed around the nanodisk with a 40-nm gap between each other. The area of each nanorod was $70\times160\,\mathrm{nm}^2$. A 150-nm-thick ITO layer coated on the glass substrate was assumed to have a refractive index of 1.55. The Au-heptamer nanostructure was fabricated using electron-beam lithography (EBL) with a deposition of 40 nm Au and 2 nm Ti served as an adhesion layer. The fabricated structures were arranged in a two-dimensional square array with a 3-μm pitch size to avoid near-field interaction between adjacent unit structures. A scanning electron microscopy (SEM) image of an isolated heptamer is presented in Fig. 1(a). In the experiment, five regions from an intact flat Au film with a large area were selected away from the heptamer to extract the photoelectron yield. The size of these five regions was the same as that extracted from the structure. Subsequently, the average value of measurements calculated to obtain the photoelectron yield of the Au flat surface was used for reference.

III. RESULTS AND DISCUSSION

The excitation of Fano resonance in the heptamer can be estimated from the simulated far-field spectrum, charge distribution, and absorption spectrum of the nanostructure [26,27]. Numerical simulation of the nanostructure was performed using the finite-difference time-domain (FDTD) method. A total-field scattered-field source was used with an incident angle of 65° with respect to the vertical axis of the sample to mimic the PEEM illumination geometry. The Au optical properties were obtained using the data presented in [28], and a refractive index of 1.55 was assumed for the ITO layer. The simulated far-field scattering and absorption spectra of the Au heptamer irradiated by s-polarized laser pulses are illustrated by the black and red curves, respectively, as illustrated in Fig. 1(b). The simulated charge distributions of the heptamer are illustrated in Fig. 1(c) for 790 nm and Fig. 1(d) for 880 nm, respectively. It can be observed that the heptamer exhibits a subradiative mode at around 790 nm [Fig. 1(c)] and a radiative mode at around 880 nm [Fig. 1(d)]. The plasmonic Fano resonance results from destructive interference between the bright plasmon and dark plasmon modes (namely, between the plasmon radiative and subradiative modes) [13]. The destructive interference between these two modes induces a Fano resonance at around 790 nm. As a result, a dip appears in the scattering spectrum around the Fano-resonance wavelength because of the strong scattering suppression by the Fano resonance. Thus, a dip and two prominent scattering peaks can be observed in the simulated scattering spectrum of the heptamer. A detailed discussion regarding the Fano resonance for a similar heptamer has been reported in previous research work [29]. Note that due to the complexity of the heptamer and the oblique incidence, the plasmon mode in the heptamer is complicated, and, overall, the heptamer exhibits a subradiative Fano resonance mode. The subradiative mode results from the cancel of the electric dipole moment among constituent units in the heptamer rather than only the subradiative quadrupole mode in the central disk. In other words, the Fano resonance is a result of the whole structure excitation instead of any isolated part of the heptamer. Additionally, the scattering spectrum presented in Fig. 1(b) indicates that the spectrum bandwidth of the radiative mode is broader than that of the subradiative mode.

It is known that the Fano-resonance effect generally produces two different kinds of phenomena: electromagnetic induced transparency (EIT) [30] and strong nanostructure absorption [16]. In the absorption mode, the photoemission can be enhanced. By contrast, in the EIT mode, a significant reduction in the photoelectron yield generally occurs [31]. In fact, these two phenomena cannot be easily distinguished by only considering the far-field scattering spectrum or charge distribution. Especially, under oblique illumination (as used in this paper), the scattering spectrum and charge distribution could be more complicated because of the emergence of retardation effects [13,32,33]. Therefore, it is necessary to obtain the absorption spectrum of the heptamer to confirm the appearance of an absorptive Fano-resonance mode. The

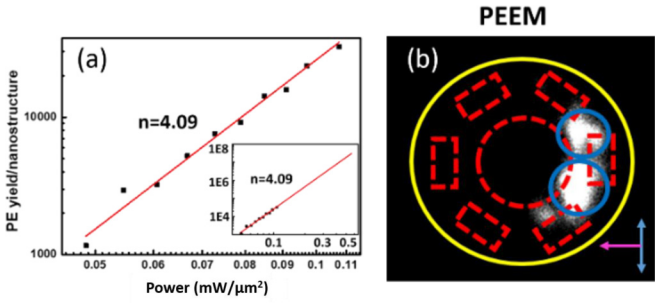

FIG. 2. (a) Photoemission electron yield of the Au heptamer as a function of the incident light power. Inset: predicted trend of the electron yield caused by an incident pulse intensity assuming four photons photoemission when the incident pulse intensity increases. (b) PEEM images of the Au-heptamer nanostructure with an 800-nm fs-laser illumination under *s*-polarization excitation. The yellow circle represents the region of the extracted electrons from a single structure.

simulated absorption spectrum of the heptamer is displayed by the red curve in Fig. 1(b). An absorption peak near 850 nm corresponding to the Fano dip in the scattering profile can be clearly observed.

The far-field spectrum peak does not accurately correspond to the near-field peak. Thus, the far-field spectrum cannot fully represent the maximum near-field enhancement [34]. By integrating the photoelectron signal and plotting it as a function of the incident laser wavelength, the wavelength-dependent photoemission (PE) intensity curve can be regarded as a near-field spectrum because the photoelectron intensity is nonlinearly correlated with the near-field intensity [20,31,35]. The normalized PE spectrum of the Au-heptamer nanostructure at oblique incidence using *s*-polarized excitation is illustrated by the red curve in Fig. 1(e). To avoid the impact of nanostructure defects, the PE-intensity curve was obtained by collecting the electrons emitted from an Au-nanostructure array. The simulated near-field enhancement in the whole structure is represented by the black curve in Fig. 1(e) that presents a peak at 790 nm. In Fig. 1(e), it can be observed that the experimental PE-curve results are consistent with the simulated near-field enhancement results. The 10-nm shift in the near-field spectrum between experimental and simulation data can be attributed to errors in the structural dimensions during EBL fabrication. It can be observed that the dip in the scattering spectrum produced by the Fano resonance [Fig. 1(b)] does not appear in the PE-yield curve in Fig. 1(e). This is because the wavelength-dependent PE yield is a comprehensive result of near-field intensity and nanostructure absorption [3,20], and its profile does not directly reflect the scattering response of the structure. The agreement among the simulated absorption spectrum, the near-field enhancement spectrum, and the experimental PE profile in Fig. 1 demonstrates that the excitation of the absorption plasmon Fano-resonance mode at 790 nm can be achieved in the heptamer.

The Fano resonance-enhanced multiphoton photoemission is demonstrated in detail in Fig. 2(a), which indicates the average photoelectron yield obtained from the heptamer using an incident laser pulse at the Fano-resonant wavelength of 800 nm. The region where the electrons are extracted from a single structure is illustrated by the yellow circle in the PEEM image of Fig. 2(b). The slope indicates that photoemission from the Au heptamer is due to a four-photon photoemission process. The photoemission yield reaches 10^4 counts at a $100\,\mu\mathrm{W}/\mu\mathrm{m}^2$ laser intensity. To confirm the photoelectron enhancement factor caused by the Fano resonance in the heptamer, the electron yield from the Au flat surface with an illumination of an 800-nm *s*-polarized femtosecond laser pulse was obtained as a reference. The collection area of the photoelectrons extracted from the Au flat surface is the same as the one depicted by the yellow circle in Fig. 2(b). It can be observed that due to the lack of plasmonic effects in the flat Au surface case, a much higher laser intensity of $I = 0.56\,m\mathrm{W}/\mu\mathrm{m}^2$ is required to ensure a reliable number of photoelectrons for reference (28 electrons were measured at $I = 0.56\,\mathrm{mW}/\mu\mathrm{m}^2$). However, it is obvious that the Au heptamer cannot be directly irradiated by laser pulses with such high intensity ($0.56\,\mathrm{mW}/\mu\mathrm{m}^2$) because of the saturation of the PEEM image. To compare the photoelectron yield at the same laser intensity, it is reasonable to extract the photoelectron yield at a laser intensity of $0.56\,\mathrm{mW}/\mu\mathrm{m}^2$ for the Au-heptamer case under the multiphoton photoemission assumption. For the case under investigation, the photoelectron yield extraction using this process is reliable because the only other possible photoelectron emission mechanism (i.e., field emission) can be eliminated based on the calculation of Keldysh parameters, as shown below.

It is known that Keldysh parameters in Eq. (1) (given below) can be used to identify the photoemission mechanism in a multiphoton regime or in a strong field regime [36]:

$$\gamma = (\omega\sqrt{2m\emptyset}/eE_1), \tag{1}$$

where ω is the laser frequency, φ is the work function of Au, $E_1 = \beta E$ is the electric-field intensity, β is the near-field enhancement factor, E is the incident electric field, and e and m are the electron charge and mass, respectively. Considering the near-field enhancement simulated using the FDTD, $\gamma \approx 3.408$ was calculated for an incident laser power density of $0.56\,\mathrm{mW}/\mu\mathrm{m}^2$. This means that it would be safe to assume that photoemission still occurs in a four-photon photoemission process, even if the incident power density is increased up to $0.56\,\mathrm{mW}/\mu\mathrm{m}^2$, as the emission mechanism is still in the range of multiphoton photoemission with $\gamma > 1$ [37]. Accordingly, the electron yield Y_{nano} of the heptamer is estimated to be 3.1×10^7 based on a four-photon photoemission process, as illustrated in the inset of Fig. 2(a). Recalling that the measured electron yield from the Au flat surface with the same area is $Y_{\mathrm{surface}} = 28$, the resulting photoemission electron yield-enhancement factor obtained from the plasmonic heptamer, which supports the Fano resonance over the Au flat surface, can be as high as $\varphi = Y_{\mathrm{nano}}/Y_{\mathrm{surface}} = 1.1\times10^6$. Hence, it can be concluded that the enhancement factor of the photoelectron yield obtained from the Fano resonance in a single Au heptamer (predicted by the measurements) can be up to six orders of magnitude higher than that of the Au flat surface under the same experimental conditions.

Notably, the photoemission electrons mainly concentrate on the right side of the heptamer (near side of the light source),

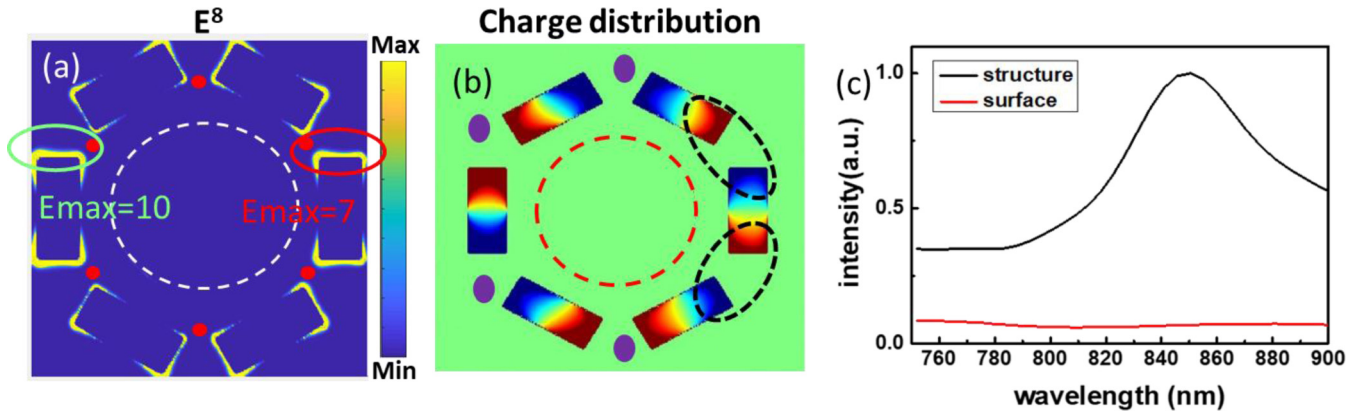

FIG. 3. (a) Simulated E^8 near-field distribution of the Au-heptamer nanostructure at 790 nm under *s*-polarization excitation. Note that E_{max} (indicated by the green and red ellipses) represents the near-field enhancement maxima within the areas before the eighth power of E (E^8). (b) Simulated charge distribution of the sample at 790 nm under *s*-polarization excitation. The dashed black ellipses and the purple dots represent areas with a strong Coulomb attraction and strong Coulomb repulsion, respectively. The charge distribution in the central disk (shown by a red dashed circle) is deliberately ignored because of the weak electric-field intensity of E^8. (c) Simulated absorption intensity spectra of the Au nanostructure (black curve) and the Au flat surface (red curve).

which is contrary to the typical case of a hot spot preferentially appearing on the far side when a nanostructure is obliquely excited by a femtosecond laser [25,32,38]. Moreover, two distinct hot spots located in the gap region (denoted by blue circles) can be observed in the PEEM image.

To further reveal the underlying mechanism of photoemission generation in the Fano-resonant nanostructure under investigation, an effort was made to reproduce the experimental PE hot-spot distribution image by simulating the E^8 near-field distribution, as illustrated in Fig. 3(a). By comparing Fig. 3(a) and Fig. 2(b), it can be observed that the simulated photoelectron distribution is somewhat different from that obtained from the experimental results; i.e., the region with a high local field (denoted by a green ellipse) is expected to emit more electrons. To identify reasons causing the difference in the PE hot-spot distribution between experiment and simulation, the charge distribution of the sample excited by an *s*-polarized 790-nm laser is displayed in Fig. 3(b). It can be observed that the hot spots in the experimental PEEM image presented in Fig. 2(b) are exactly located in the gap region with strong Coulomb attraction [as depicted by the black dashed ellipses in Fig. 3(b)]. Meanwhile, by comparing Figs. 2(b) and 3(b), it can be observed that there is almost no photoemission from the gap region [denoted by the purple dots in Fig. 3(b)] with strong Coulomb repulsion, even though the corners of the surrounding bars exhibit high charge density. The Coulomb effects on PE can be explained as follows. The Coulomb attraction provides oscillating electrons with an additional force pointing out of the nanostructures. This force makes the electrons escape from the nanostructures, thus inducing strong photoemission. By contrast, Coulomb repulsion provides oscillating electrons with an additional force pointing into the nanostructures, thus preventing photoelectron emission.

Next, the contributions of both local-field enhancement [the near-field region corresponding only to the Coulomb attraction area is considered, as indicated by the black dashed ellipses in Fig. 3(b)] and strong absorption due to the Fano resonance are evaluated. These two are considered to be the main factors contributing to the multiphoton photoemission [3]. It is generally accepted that the multiphoton photoemission yield is proportional to the plasmonic near-field intensity on the upper surface [39,40]. Accordingly, the photoemission yield-enhancement factor obtained from the FDTD simulated electric-field enhancement on the nanostructure upper surface was estimated. This factor was compared to that obtained for the flat surface, where the integration was performed over the region marked by the yellow circle in Fig. 2(b). The integration included the entire nanostructure surface; S_f and E_f are the area and the electric-field intensity of the flat surface, respectively [3]. The calculated results indicate that the photoelectron enhancement factor arising from the local-field enhancement at the upper surface is approximately 628 times larger than that at the flat surface. Additionally, the strong Au-heptamer absorption induced by the Fano resonance is another factor responsible for photoemission enhancement. The absorption spectra of the nanostructure and the flat surface are illustrated in Fig. 3(c). The absorption parameters were substituted into the generalized Fowler-Dubridge equation [41], and the predicted photoelectron yield enhancement due to the strong absorption was $Y_{FD} = A^4_{nano}/A^4_{surface} = 2.68\times10^2$. Here A_{nano} and $A_{surface}$ correspond to the nanostructure and flat surface absorptions, respectively. Therefore, by combining the contributions from both effects (strong absorption and near-field enhancement at the upper surface of the heptamer), a total photoelectron yield-enhancement factor of 1.68×10^5 was obtained. Obviously, the calculated PE-enhancement factor of the upper structure surface is much lower than the experimental PE-enhancement factor of 1.1×10^6. Therefore, it can be concluded that the photoelectrons are not mainly emitted from the upper surface of the heptamer.

The unexpected photoelectron emission position observed in the PEEM image and the much lower calculated PE yield from the upper surface with respect to the experimental measurements indicate that there are other pathways for photoelectron emission. It is known that the photoelectrons emitted from a plasmonic nanostructure are possibly ejected from the ITO substrate or from the junction region between

the lower surface of the nanostructure and ITO substrate [42,43]. Naturally, it is reasonable to assume that the photoelectron emission from the ITO surface is due to direct exposure to laser irradiation and plasmonic energy transfer from Au to ITO [42]. However, since the work function value of ITO is close to 4.1 eV, the photoelectron nonlinear order should be 3 under 800-nm (1.55-eV) pulse irradiation. This result is in contrast to the measured four-photon photoemission process illustrated in Fig. 2(a). It is obvious that the photoelectrons in this study are still emitted from several points in the Au nanostructure. The other photoemission pathway originates from the junction region between the nanostructure's lower surface and the ITO substrate, and the near-field enhancement on the lower surface is generally higher than that on the upper surface [43]. The electric-field intensity in the region that is above 2 nm from the sample's lower surface was simulated at a 790-nm excitation. The results indicate that the enhancement factor of the photoelectrons induced by the electric-field enhancement in these areas is approximately 7.58×10^3. Considering the 2.68×10^2 absorption contribution, an enhancement factor of 2.1×10^6 over the Au flat surface can be obtained. This is in agreement with the experimental results. The foregoing results suggest that the observed photoelectrons are mainly emitted from the junction region between the nanostructure's lower surface and the ITO substrate. Similar phenomena (photoelectrons emitted from the junction region) have also been observed by other research groups [22,43].

To further demonstrate the advantage of Fano resonance-enhanced multiphoton photoemission, the PE enhancement achieved by the nanostructure with the Fano excitation was compared with that achieved by the nanostructure with the non-Fano excitation. The simulated far-field scattering spectrum of the Au heptamer illuminated under a *p*-polarization excitation is presented in Fig. 4(a). In this figure, no clear Fano-resonant profile can be observed. The PEEM image and charge distribution of the structure are presented in Figs. 4(b) and 4(c), respectively. By recording the photoemission electron yields of the Au flat surface and the heptamer nanostructure under *p*-polarized light illumination and comparing with the case of the *s*-polarized light illumination, it can be deduced that PE enhancement under *s* polarization (with Fano-resonance excitation) is 197 times higher than that under *p*-polarization (with non-Fano plasmon excitation).

The influence of the Coulomb effects on photoemission can also be observed under a *p*-polarization light excitation. Figures 4(b) and 4(c) indicate that exactly the same influence of the Coulomb effects on photoemission can be observed under a *p*-polarization excitation with that of an *s*-polarization excitation. The PEEM image of the sample with a *p*-polarization light excitation is presented in Fig. 4(b). It can be observed that the hot spots appear at the upper and lower positions [denoted by the blue ellipses in Fig. 4(b)]. By comparing Figs. 4(b) and 4(c), it can be observed that the PE hot spots are located in the regions corresponding to strong Coulomb attraction [denoted by the black dash circles in Fig. 4(c)]. Additionally, there is almost no photoemission from the gap region with Coulomb repulsion [denoted by the purple dots in Fig. 4(c)]. These results clearly demonstrate that the Coulomb

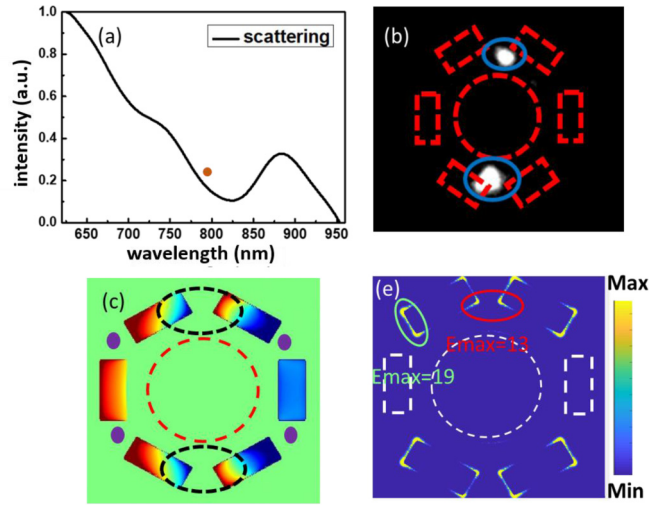

FIG. 4. (a) Simulated far-field scattering spectrum of the sample under a *p*-polarization excitation. The brown dot indicates the corresponding wavelength of the charge distribution shown in (c). (b) PEEM image of the Au-heptamer nanostructure under a *p*-polarized 800-nm fs-laser illumination. (c) Simulated charge distribution of the sample under a *p*-polarized 790-nm excitation. The dashed black ellipses and the purple dots represent the gap areas with strong Coulomb attraction and strong Coulomb repulsion, respectively. (e) Simulated near-field E^8 distribution of the Au-heptamer nanostructure at 790 nm under a *p*-polarization excitation. Note that E_{max} denoted by green and red circles represents the maxima of near-field enhancement within the regions before the eighth power of E (E^8).

effect has a strong impact on photoemission in this heptamer structure.

It can be observed that the hot spots observed in the PEEM images under *s* polarization [Fig. 2(b)] and *p*-polarization [Fig. 4(b)] excitations correspond to the aligned split-dipole antenna producing great local-field enhancement. This observation seems to suggest that the aligned nanorod dimer model is responsible for the observed hot spots in the PEEM image due to the high local-field enhancement. After carefully checking the local-field enhancement in the heptamer, other positions with even higher local-field intensities in the heptamer [denoted by the green circles in the near-field distribution in Figs. 3(a) and 4(d)] can be observed. However, no hot spots appear to emanate from these positions, which exhibit a much stronger local field. Therefore, the split-dipole antenna model is incapable of explaining the experimental results obtained.

To further confirm that the split nanorod dimer model is incapable of interpreting the observed PEEM images, a further experiment with the hexamer (which is formed by only removing the central disk from the heptamer and leaving the remaining parameters unchanged) was performed. An SEM image of the hexamer is presented in Fig. 5(a). The scattering and absorption hexamer spectra are presented in Fig. 5(b). It can be observed that the scattering and absorption peaks of the structure appear at around 790 nm, which does not correspond to the Fano resonance. The calculated E^8 of this structure is illustrated in Fig. 5(c), and the maximum near-field enhancement (denoted by green circles) is shown on the

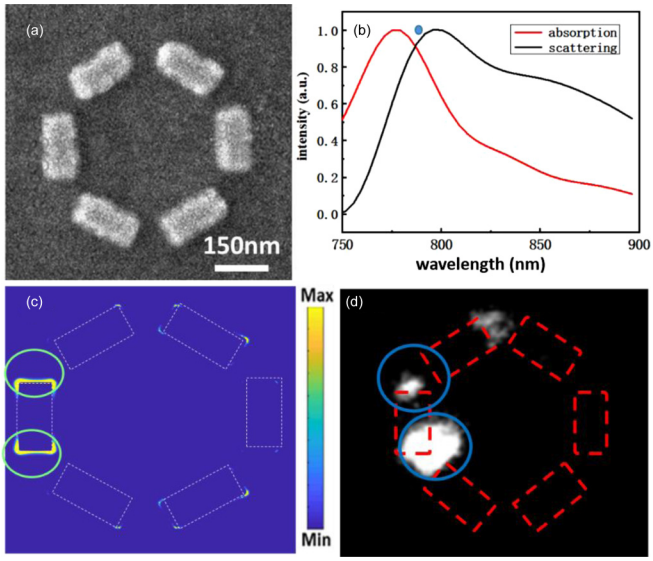

FIG. 5. (a) SEM image of the Au hexamer [the central disk has been removed from the heptamer in Fig. 1(a)]. (b) Simulated far-field scattering and absorption spectrum of the hexamer. (c) Simulated near-field E^8 distribution of the Au hexamer at 790 nm under an *s*-polarization excitation. (d) PEEM images of the Au hexamer with an illumination of 800-nm fs laser under *s* polarization.

left of the structure. The experimental PEEM image of the hexamer illuminated by an 800-nm laser pulse is presented in Fig. 5(d). It is clearly observed that the hot spots appear on the left side of the structure, which is quite different from the PEEM image of the heptamer supporting the Fano resonance, as illustrated in Fig. 2(b), where the hot spots appear on the right side of the structure. Therefore, the missing central disk has a large impact on the photoemission. The experimental results demonstrate that the central disk plays a key role in the photoemission of the heptamer structure, and the split nanorod dimer model is incapable of interpreting the observed PEEM images. This suggests that the plasmon Fano-resonant mode is critical to the photoelectron enhancement in the heptamer.

IV. CONCLUSIONS

In summary, it was demonstrated that a significant (six orders of magnitude) photoemission enhancement from a heptamer supporting the Fano-resonant mode over an Au flat surface can be achieved. The experimental results were supported by calculations, considering the strong absorption and local near-field enhancement effects. The experimental results, which were assisted with FDTD simulation and calculations, revealed that the photoelectrons are mainly emitted from the junction area between the lower surface of the Au heptamer and the ITO film on the substrate rather than the upper surface of the nanostructure. Moreover, it was found that the photoelectrons are emitted from regions with strong Coulomb attraction rather than from regions with Coulomb repulsion, even though the latter exhibits higher near-field intensity. Our findings provide a deep understanding of the multiphoton photoemission mechanism in a plasmonic Fano-resonant nanostructure, thus offering a platform to explore the energy exchange between plasmons and electrons, eventually paving the way for potential photoelectron-based devices.

ACKNOWLEDGMENTS

This project was supported by the National Natural Science Foundation of China (NSFC) (Grants No. 61775021, No. 91850109, No. 11474040, No. 62005022, and No. 12004052), Education Department of the Jilin Province (Grant No. JJKH20190555KJ), Department of Science and Technology of the Jilin Province (Grants No. 20200201268JC and No. 20200401052GX), "111" Project of China (Grant No. D17017), Youth Fund of CUST (Grant No. XQNJJ-2018-02), China Postdoctoral Science Foundation (Grant No. 2019M661183), and the Ministry of Education Key Laboratory for Cross-Scale Micro and Nano Manufacturing, Changchun University of Science and Technology.

[1] W. L. Barnes, A. Dereux, and T. W. Ebbesen, Nature (London) **424**, 824 (2003).
[2] A. V. Kabashin, P. Evans, S. Pastkovsky, W. Hendren, G. A. Wurtz, R. Atkinson, R. Pollard, V. A. Podolskiy, and A. V Zayats, Nat. Mater. **8**, 867 (2009).
[3] R. K. Li, H. To, G. Andonian, J. Feng, A. Polyakov, C. M. Scoby, K. Thompson, W. Wan, H. A. Padmore, and P. Musumeci, Phys. Rev. Lett. **110**, 074801 (2013).
[4] A. Polyakov, C. Senft, K. F. Thompson, J. Feng, S. Cabrini, P. J. Schuck, H. A. Padmore, S. J. Peppernick, and W. P. Hess, Phys. Rev. Lett. **110**, 076802 (2013).
[5] R. G. Hobbs, Y. Yang, A. Fallahi, P. D. Keathley, E. De Leo, F. X. Kärtner, W. S. Graves, and K. K. Berggren, ACS Nano **8**, 11474 (2014).
[6] W. P. Putnam, R. G. Hobbs, P. D. Keathley, K. K. Berggren, and F. X. Kartner, Nat. Phys. **13**, 335 (2017).
[7] P. Dombi, A. Hörl, P. Rácz, I. Márton, A. Trügler, J. R. Krenn, and U. Hohenester, Nano Lett. **13**, 674 (2013).
[8] P. M. Nagel, J. S. Robinson, B. D. Harteneck, T. Pfeifer, M. J. Abel, J. S. Prell, D. M. Neumark, R. A. Kaindl, and S. R. Leone, Chem. Phys. **414**, 106 (2013).
[9] Y. Gong, A. G. Joly, L. M. Kong, P. Z. El-Khoury, and W. P. Hess, Phys. Rev. Appl. **2**, 064012 (2014).
[10] A. Feist, N. Bach, N. Rubiano da Silva, T. Danz, M. Möller, K. E. Priebe, T. Domröse, J. G. Gatzmann, S. Rost, J. Schauss, S. Strauch, R. Bormann, M. Sivis, S. Schäfer, and C. Ropers, Ultramicroscopy **176**, 63 (2017).
[11] E. Quinonez, J. Handali, and B. Barwick, Rev. Sci. Instrum. **84**, 103710 (2013).
[12] P. Musumeci, L. Cultrera, M. Ferrario, D. Filippetto, G. Gatti, M. S. Gutierrez, J. T. Moody, N. Moore, J. B. Rosenzweig, C. M. Scoby, G. Travish, and C. Vicario, Phys. Rev. Lett. **104**, 084801 (2010).
[13] B. Luk'yanchuk, N. I. Zheludev, S. a Maier, N. J. Halas, P. Nordlander, H. Giessen, and C. T. Chong, Nat. Mater. **9**, 707 (2010).

[14] J. Cui, B. Ji, X. Song, and J. Lin, Plasmonics **14**, 41 (2019).
[15] Z. Qiang, W. Zhou, M. Lu, and G. J. Brown, Proc. SPIE **6901**, 69010F (2008).
[16] M. Yorulmaz, A. Hoggard, H. Zhao, F. Wen, W. S. Chang, N. J. Halas, P. Nordlander, and S. Link, Nano Lett. **16**, 6497 (2016).
[17] C. Wu, A. B. Khanikaev, R. Adato, N. Arju, A. A. Yanik, H. Altug, and G. Shvets, Nat. Mater. **11**, 69 (2011).
[18] S. J. Peppernick, A. G. Joly, K. M. Beck, and W. P. Hess, J. Chem. Phys. **138**, 154701 (2013).
[19] M. Dabrowski, Y. Dai, A. Argondizzo, Q. Zou, X. Cui, and H. Petek, ACS Photon. **3**, 1704 (2016).
[20] Y. Li, Q. Sun, S. Zu, X. Shi, Y. Liu, X. Hu, K. Ueno, Q. Gong, and H. Misawa, Phys. Rev. Lett. **124**, 163901 (2020).
[21] G. Spektor, D. Kilbane, A. K. Mahro, B. Frank, S. Ristok, L. Gal, P. Kahl, D. Podbiel, S. Mathias, H. Giessen, F.-J. M. zu Heringdorf, M. Orenstein, and M. Aeschlimann, Science **355**, 1187 (2017).
[22] Y. Dai, M. Dabrowski, and H. Petek, J. Chem. Phys. **152**, 054201 (2020).
[23] D. Podbiel, P. Kahl, A. Makris, B. Frank, S. Sindermann, T. J. Davis, H. Giessen, M. H. Von Hoegen, and F. J. M. Zu Heringdorf, Nano Lett. **17**, 6569 (2017).
[24] E. Mårsell, A. Losquin, R. Svärd, M. Miranda, C. Guo, A. Harth, E. Lorek, J. Mauritsson, C. L. Arnold, H. Xu, A. L'Huillier, and A. Mikkelsen, Nano Lett. **15**, 6601 (2015).
[25] B. Ji, J. Qin, H. Tao, Z. Hao, and J. Lin, New J. Phys. **18**, 093046 (2016).
[26] J. A. Fan, K. Bao, C. Wu, J. Bao, R. Bardhan, N. J. Halas, V. N. Manoharan, G. Shvets, P. Nordlander, and F. Capasso, Nano Lett. **10**, 4680 (2010).
[27] J. A. Fan, C. Wu, K. Bao, J. Bao, R. Bardhan, N. J. Halas, V. N. Manoharan, P. Nordlander, G. Shvets, and F. Capasso, Science **328**, 1135 (2010).
[28] P. B. Johnson and R. W. Christy, Phys. Rev. B **6**, 4370 (1972).
[29] P. Alonso-Gonzalez, M. Schnell, P. Sarriugarte, H. Sobhani, C. Wu, N. Arju, A. Khanikaev, F. Golmar, P. Albella, L. Arzubiaga, F. Casanova, L. E. Hueso, P. Nordlander, G. Shvets, and R. Hillenbrand, Nano Lett. **11**, 3922 (2011).
[30] S. Zhang, D. A. Genov, Y. Wang, M. Liu, and X. Zhang, Phys. Rev. Lett. **101**, 047401 (2008).
[31] H. Yu, Q. Sun, K. Ueno, T. Oshikiri, A. Kubo, Y. Matsuo, and H. Misawa, ACS Nano **10**, 10373 (2016).
[32] B. Ji, X. Song, Y. Dou, H. Tao, X. Gao, Z. Hao, and J. Lin, New J. Phys. **20**, 073031 (2018).
[33] B. Ji, Q. Wang, X. Song, H. Tao, Y. Dou, X. Gao, Z. Hao, and J. Lin, J. Phys. D: Appl. Phys. **50**, 415309 (2017).
[34] J. Zuloaga and P. Nordlander, Nano Lett. **11**, 1280 (2011).
[35] H. Yu, Q. Sun, J. Yang, K. Ueno, T. Oshikiri, A. Kubo, Y. Matsuo, Q. Gong, and H. Misawa, Opt. Express **25**, 6883 (2017).
[36] L. V. Keldysh, Sov. Phys. JETP **20**, 1307 (1965).
[37] C. Li, X. Zhou, F. Zhai, Z. Li, F. Yao, R. Qiao, K. Chen, M. T. Cole, D. Yu, Z. Sun, K. Liu, and Q. Dai, Adv. Mater. **29**, 1701580 (2017).
[38] P. Lang, X. Song, B. Ji, H. Tao, Y. Dou, X. Gao, Z. Hao, and J. Lin, Opt. Express **27**, 6878 (2019).
[39] P. Melchior, D. Bayer, C. Schneider, A. Fischer, M. Rohmer, W. Pfeiffer, and M. Aeschlimann, Phys. Rev. B **83**, 235407 (2011).
[40] R. G. Hobbs, W. P. Putnam, A. Fallahi, Y. Yang, F. X. Kärtner, and K. K. Berggren, Nano Lett. **17**, 6069 (2017).
[41] J. H. Bechtel, W. Lee Smith, and N. Bloembergen, Phys. Rev. B **15**, 4557 (1977).
[42] R. C. Word, T. Dornan, and R. Könenkamp, Appl. Phys. Lett. **96**, 251110 (2010).
[43] J. Yang, Q. Sun, H. Yu, K. Ueno, H. Misawa, and Q. Gong, Photon. Res. **5**, 187 (2017).